# Band Offsets of Metal Oxide Contacts on TlBr Radiation Detectors

Olivia K. Voyce,[1,2] Mark A. Isaacs,[3,4] Laura J. Harkness-Brennan,[1]
Tim D. Veal,[1,2,*] Dan S. Judson,[1] Shariar Motakef,[5] and Amlan Datta[5]

[1] *Oliver Lodge Laboratory, Department of Physics, University of Liverpool, L69 7ZE, United Kingdom*
[2] *Stephenson Institute for Renewable Energy, University of Liverpool, L69 7ZF, United Kingdom*
[3] *HarwellXPS, Research Complex at Harwell, RAL, Didcot OX11 0FA, United Kingdom*
[4] *Department of Chemistry, University College London, WC1H 0AJ*
[5] *CapeSym, Inc., Natick, MA 01760, USA*

(Dated: October 10, 2021)

Metal oxides are investigated as an alternative to metal contacts on thallium bromide (TlBr) radiation detectors. X-ray photoelectron spectroscopy studies of $SnO_2$/TlBr and ITO/TlBr devices indicate that a type-II staggered heterojunction forms between TlBr and metal oxides upon contacting. By using the Kraut method of valence band offset (VBO) determination, the VBOs of $SnO_2$/TlBr and ITO/TlBr heterojunctions are determined to be 1.05 ± 0.17 eV and 0.70 ± 0.17 eV, respectively. The corresponding conduction band offsets (CBO) are then found to be 0.13 ± 0.17 eV and 0.45 ± 0.17 eV respectively. The I-V response of symmetric In/$SnO_2$/TlBr and In/ITO/TlBr planar devices is almost Ohmic with leakage current of less than 2.5 nA at 100 V.

## I. INTRODUCTION

Thallium bromide (TlBr) is a promising material for the handheld detection of gamma rays, owing to its large band gap (2.68 eV), high resistivity and stopping power [1]. At room temperature, however, TlBr undergoes ionic polarization when subject to an external electric field [2–4]. It has been suggested that the primary effect of polarization is the migration of the $Br^-$ ions towards the anode through the mechanism of vacancy hopping [4], and their subsequent reaction with the metallic anode material. The reaction of the metal anode with the migrating $Br^-$ ions can produce metal bromide reaction products under the electrode [3]. If the device is under prolonged bias, the metal electrode can be corroded until it is virtually impossible to apply any electric field, leading to total device failure [4, 5].

Reducing the reaction of the $Br^-$ ions with the electrode material has been the focus of a large body of TlBr research. Approaches include chemically treating the TlBr crystal to reduce defects at the surface [6, 7] altering the electronic structure at the interface [8, 9] and determining the optimal metallic electrode material [10]. The use of thallium contacts has shown promising results, with extended lifetimes of over 10,000 hours being reported [11, 12]. However, this often has to be used in tandem with bias switching techniques, which are not readily deployed for in-situ radioactive assay.

A recent study [13] has reported that the use of metal oxide electrodes results in stable and low noise detection of gamma rays for more than 4000 hours when under unidirectional bias. This paper explores the use of metal oxide electrodes further by using x-ray photoelectron spectroscopy (XPS) and the Kraut method to determine the valence band offset and resulting heterojunction at the contact/TlBr interface [14].

## II. METHODS

Four TlBr crystals were used in this study. They were grown at CapeSym, Inc. using the travelling molten zone technique as reported in Ref. 5. The crystals were cut to a size of 6.5 × 6.5 × 1.5 $mm^3$ using a diamond wire saw. The samples were then cleaned using acetone in an ultrasonic bath for 20 minutes to remove any debris left from the cutting procedure. One crystal, labelled 'Uncontacted TlBr' in Table I, underwent no further processing after this stage. The remaining three samples were then chemo-mechanically polished. This was achieved by grinding them on SiC paper whilst simultaneously etching with a $HBr:H_2O_2:H_2O$ (1:1:5) solution. The samples subsequently underwent fine polishing and smooth etching in a fresh batch of the $HBr:H_2O_2:H_2O$ solution. Standard tabulated reduction potentials [15], indicate that $H_2O_2$ would be expected to oxidise HBr and so the mixture is thermodynamically unstable. However, at room temperature the solution is kinetically stable. The polished surfaces were rinsed in methanol and dried in air.

The In/TlBr, $SnO_2$/TlBr and ITO/TlBr samples had ∼ 2 nm of thermally evaporated indium, thermally evaporated $SnO_2$ or sputtered ITO onto its surface after processing. The $SnO_2$/TlBr and ITO/TlBr samples also had ∼ 2 nm of indium metal deposited on top of the metal oxide layer. This is a typical device structure for radiation devices as the indium overlayer provides a good connection between the bonding wire and electrode [13]. The contact area for all three samples was 5×5 $mm^2$. Thicker films of $SnO_2$ and ITO were also used in the Kraut method valence band offset determination [14].

XPS measurements were performed on as-received samples at HarwellXPS, using a Thermo Fisher Scientific

* T.Veal@liverpool.ac.uk

TABLE I. Details of the selected samples used in the XPS study; including contact type, deposition method and thickness.

| Sample | Deposition Type | Thickness (nm) |
|---|---|---|
| Uncontacted TlBr | ... | ... |
| In/TlBr | Thermal Evaporation | 2 ± 0.1 |
| $SnO_2$/TlBr | Thermal Evaporation | 2 ± 0.1 |
| ITO/TlBr | Sputtering | 2 ± 0.1 |
| Thick ITO[a] | Sputtering | 220 ± 30 |
| Thick $SnO_2$[b] | CVD | 350 ± 20 |

[a] A thick ITO film was deposited on glass by Zhuhai Kaivo Optoelectronic Technology Co, Ltd.

[b] A thick fluorine-doped $SnO_2$ film was grown on soda lime glass by chemical vapour deposition (CVD) at atmospheric pressure by the NSG group.

NEXSA spectrometer with a micro-focused monochromatic Al K$\alpha$ source (hv=1486.6 eV) and an x-ray source power of 150 W. Spectra were collected with a pass energy of 40 eV and a resolution of 0.47 eV. The resolution was determined by measuring the width of the Fermi edge of a polycrystalline gold reference sample at room temperature. A low-energy electron flood gun was used for charge neutralization of the low-conductivity TlBr sample.

Absolute energy calibration is not needed for the determination of a VBO using the Kraut method [14]. However, for the purpose of reporting core level positions, the binding energies were calibrated with reference to the Au Fermi level. The uncontacted TlBr sample had charged and therefore data relating to this sample was shifted based on the average C 1$s$ values of the uncharged samples. The Tl 4$f$, Br 3$p$, In 3$d$ and Sn 3$d$ core level (CL) peaks were fitted using Shirley background and Voigt (60–70%/40–30% mixed Lorentzian-Gaussian) line shapes. The position of the valence band maximum (VBM) was determined by extrapolating a linear fit to the leading edge of the valence band spectra to the background level.

## III. RESULTS

XPS measurements of the Br 3$p$ doublet, Tl 4$f$ doublet and VBM region for the uncontacted TlBr sample are shown in Figures 1a, 1b and 1c, respectively. The Tl 4$f$ region was fitted using one doublet, with a spin orbit separation of $\Delta E_{SO}$=4.43 eV and an area ratio of 4:3. The Tl $4f_{7/2}$ peak component was found to have a binding energy of 118.94 ± 0.05 eV. The Br 3$p$ region was fitted using one doublet, with a spin orbit separation of $\Delta E_{SO}$ = 6.7 eV and an area ratio of 2:1. The Br $3p_{3/2}$ peak component was found to have a binding energy of 181.69 ± 0.05 eV. The valence band maximum of the uncontacted TlBr sample was determined to be 1.6 ± 0.1 eV. The parameters of all fitted regions are displayed in Table II. The Tl $4f_{7/2}$ component is consistent with literature reported values for the Tl-Br bond [9, 16]. As both the Tl 4$f$ and Br 3$p$ regions could only sensibly fitted using one component each, it was inferred that they both arose from the Tl-Br bond. The absence of any further components suggests that under atmospheric conditions, the surface of the TlBr crystal has not oxidised. Spectra for the Tl 4$d$ and Br 3$d$ peaks were also collected, and no evidence was found from them to contradict this interpretation. The binding energy values presented here for the TlBr components of the Tl 4$f$ and Br 3$p$ peaks were used in the analysis of the XPS data from the metal and metal oxide-contacted TlBr samples.

Figures 2a and 2b display the Br 3$p$ and Tl 4$f$ regions for the In/TlBr sample, respectively. The Tl 4f region was fitted using two doublets associated with the Tl 4$f$ peak in addition to an In 4$s$ component at 123.80 ± 0.05 eV. It is likely that there were multiple indium components present; however the broad nature of the In 4$s$ component meant that they were unresolvable. The Br 3$p$ component was found to have a binding energy of 182.33 ± 0.05 eV and the two Tl $4f_{7/2}$ components were found to have binding energies of 119.68 ± 0.05 eV and 117.90 ± 0.05 eV. The Br 3$p$ component and higher energy Tl 4$f$ component were associated with the Tl-Br bond. Both components are slightly higher than that found for the Tl-Br bond in the TlBr sample, but this could be due to a change in the electronic environment of the crystal atoms upon application of the contact material at the interface.

The lower binding energy Tl 4$f$ component was associated with the presence of $Tl_2O_3$, possibly produced during the etching process when TlBr reacts with $H_2O_2$. The presence of a small amount of $Tl_2O_3$ on the surface of the etched and indium-contacted TlBr and its absence from the unetched TlBr surface, suggests that $Tl_2O_3$ results from the strong oxidising effect of $H_2O_2$. While, according to tabulated standard reduction potentials [15], the reaction $2TlBr + 3H_2O_2 \rightarrow Tl_2O_3 + Br_2 + 3H_2O$ is indeed thermodynamically allowed, the concentration is small according to the low relative intensity of the $Tl_2O_3$-related Tl 4f peaks. This represents an unusual situation where the higher oxidation state component ($Tl^{3+}$) is at a lower binding energy than the $Tl^+$ component resulting from the Tl-Br bond, but has previously been reported [17]. The binding energy separation between the two Tl $4f_{7/2}$ components was calculated to be 1.78 ± 0.07 eV. This is consistent with the separation between TlBr and $Tl_2O_3$ reported in Ref. 16. The binding energy of the Tl $4f_{7/2}$ $Tl_2O_3$ component is also consistent with values reported in by Glans *et al.* [17]. Here, strong satellites are observed in $Tl_2O_3$ due to the presence of a conduction band plasmon (CBP) loss feature, typically present in metal oxides with high doping levels, as reported by Egdell *et al.* [18, 19]. These are not observed in the Tl 4$f$ region presented in this paper. Their presence cannot be discounted, however, as the $Tl_2O_3$ plasmons may not be observable due to differences between the likely amorphous $Tl_2O_3$ formed at the surface of the TlBr crystal and the crystalline $Tl_2O_3$ studied by Glans *et al.* The

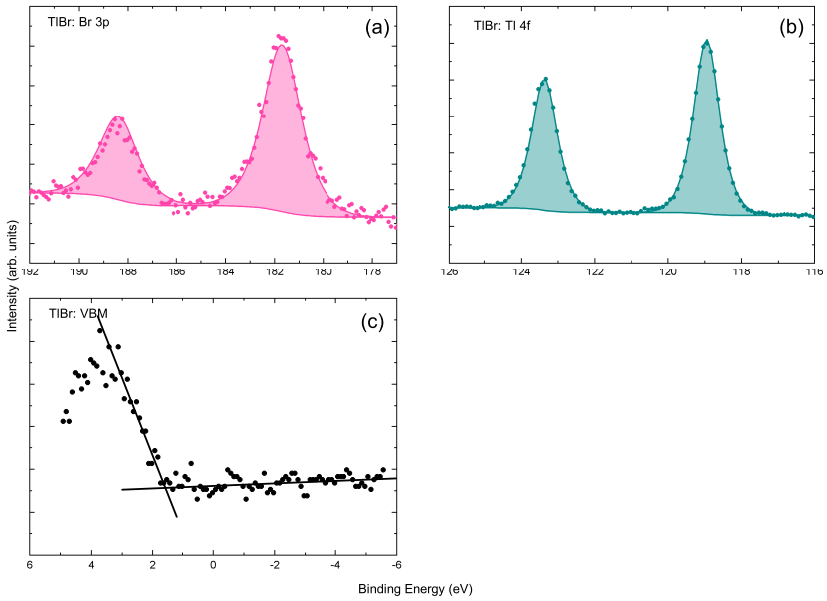


FIG. 1. (a) Br 3$p$ core level peaks, (b) Tl 4$f$ core level peaks, and (c) valence band photoemission spectrum for the uncontacted TlBr sample.

plasmon lifetime may be very short and result in a broad and flat CBP component. Furthermore, the $Tl_2O_3$ components reported here are only a small contribution to the intensity of the peaks (TlBr: 98.14 %, $Tl_2O_3$: 1.86 %), which could make the core level and CBP peaks difficult to resolve.

Figure 3b shows the Tl 4$f$ doublet for the $SnO_2$/TlBr sample. This was fitted by a single doublet associated with the Tl 4$f$ core level in addition to a broad In 4$s$ component. The In 4$s$ had a binding energy of 123.67 eV, which was consistent with the In 4$s$ component in the In/TlBr sample. The Tl $4f_{7/2}$ component was found to have a binding energy of 119.51 eV, which was consistent with the Tl-Br bond presented in the In/TlBr sample. There are no $Tl_2O_3$ peaks evident in this region, however this could be due to the large tail of the broad In 4s peak masking the low intensity peaks. It is therefore still possible that $Tl_2O_3$ is present to a small extent on the $SnO_2$/TlBr surface due to the chemical etch, in the same way as the In/TlBr sample.

A comparison of the Sn 3$d$ regions from the $SnO_2$/TlBr and thick $SnO_2$ samples can be seen in Figures 3a and 3c, respectively. The Sn 3$d$ core level peaks were fitted using two doublets for both samples. Each doublet had a spin orbit splitting of $\Delta E_{SO}$=8.41 eV [20] and an area ratio of 3:2. The lower binding energy component is associated with the $SnO_2$ bonding, whilst the higher energy component is thought to correspond to a CBP loss feature. Assignment of peaks in this way, for fluorine doped $SnO_2$ films, has previously been performed by Swallow *et al.* [21] with results consistent to those presented here. The VBM region for the thick $SnO_2$ sample is presented in Figure 3d. The VBM position was found to be 3.7 ± 0.1 eV with respect to the Fermi level.

Figure 4b shows the Tl 4$f$ doublet for the ITO/TlBr sample. In a similar way to the $SnO_2$/TlBr sample, this region was fitted using a single doublet associated with the Tl 4$f$ core level well as a broad In 4s component at 123.46 ± 0.05 eV. The Tl 4$f$ component at 119.64 ± 0.05 eV is consistent with the binding energies for the Tl-Br bonding identified in both the In/TlBr and $SnO_2$-contacted samples. Again, there were no $Tl_2O_3$ components measured but this could be due to the large intensity of the In 4s component.

The In 3$d$ regions for the ITO/TlBr and thick ITO samples are presented in Figures 4a and 4c, respectively. The In 3$d$ core level peaks were fitted using two doublets for both samples, with a spin orbit splitting of $\Delta E_{SO}$= 7.52 eV and an area ratio of 3:2 for each doublet [20]. Here, the lower binding energy component was identified as $In_2O_3$ and the higher binding energy component as due to CBP losses. The VBM region for the thick ITO sample is presented in Figure 4d. The VBM was found to be at 3.4 ± 0.1 eV below the Fermi level.

In order to assess the efficacy of metal oxide contacts on TlBr detectors, it is important to determine the band line up at the interface. The valence band offsets were

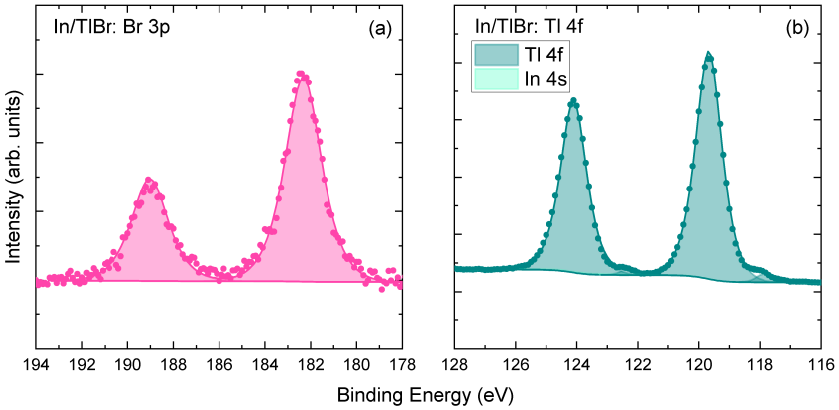


FIG. 2. (a) Br $3p$ core level peaks and (b) Tl $4f$ core level peaks for the In/TlBr sample.

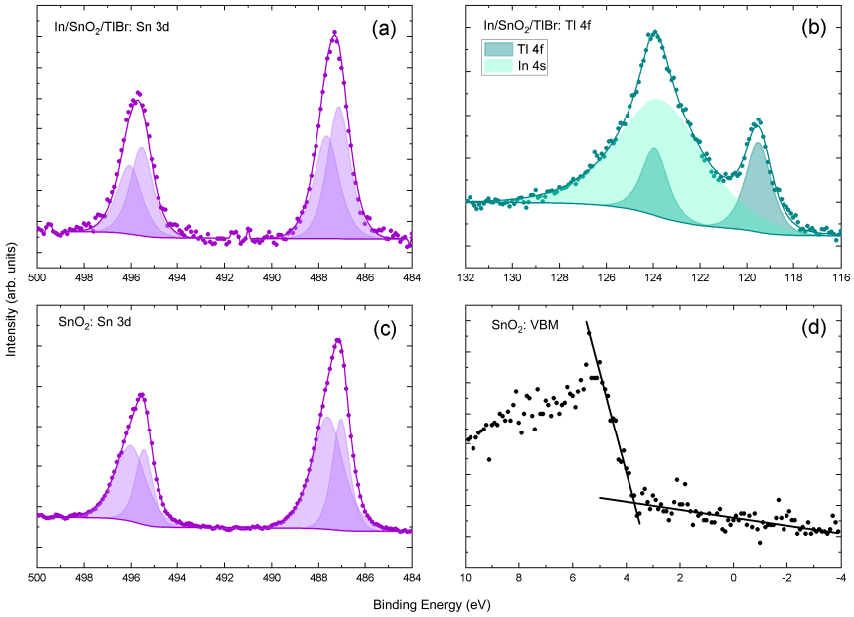


FIG. 3. (a) Sn $3d$ core level peaks and (c) Tl $4f$ core level peaks for the $SnO_2$/TlBr sample as well as the (b) Sn $3d$ core level peak and (d) valence band photoemission spectrum for the thick $SnO_2$ sample.

determined using the Kraut [14] method:

$$\Delta E_v = \Delta E_{CL} + \left(E^B_{CL} - E^B_V\right) - \left(E^A_{CL} - E^A_V\right) \qquad (1)$$

where $E^A_V$ and $E^A_{CL}$ refer to the VBM and core level energies in a bulk TlBr sample and $E^B_V$ and $E^B_{CL}$ refers to the VBM and core level energies in either the thick $SnO_2$ or ITO sample. $\Delta E_{CL}$ is the separation between the Tl $4f$ and either Sn 3d or In $3d$ component, in the $SnO_2$/TlBr or ITO/TlBr, respectively. By using the TlBr component in the Tl $4f$ core level peak and the $SnO_2$ component of the Sn 3d peak, the valence band offset for the sample $SnO_2$/TlBr was calculated to be 1.05 ± 0.17 eV. By using the $In_2O_3$ component of the In 3d peak, the valence band offset for the sample ITO/TlBr was calculated to be 0.70 ± 0.17 eV. These calculated offsets, in addition to room temperature band gaps for TlBr (2.68 eV [1]), $In_2O_3$ (2.93 eV [22]) and $SnO_2$ (3.60 eV [23]) allow the heterojunction band structure to be determined, as shown in Figure 5. Both the ITO and $SnO_2$ metal oxide contacts form a type-II staggered heterojunction when deposited on TlBr.

The I-V characteristics of 6.5×6.5×1.5 $mm^3$ symmet-

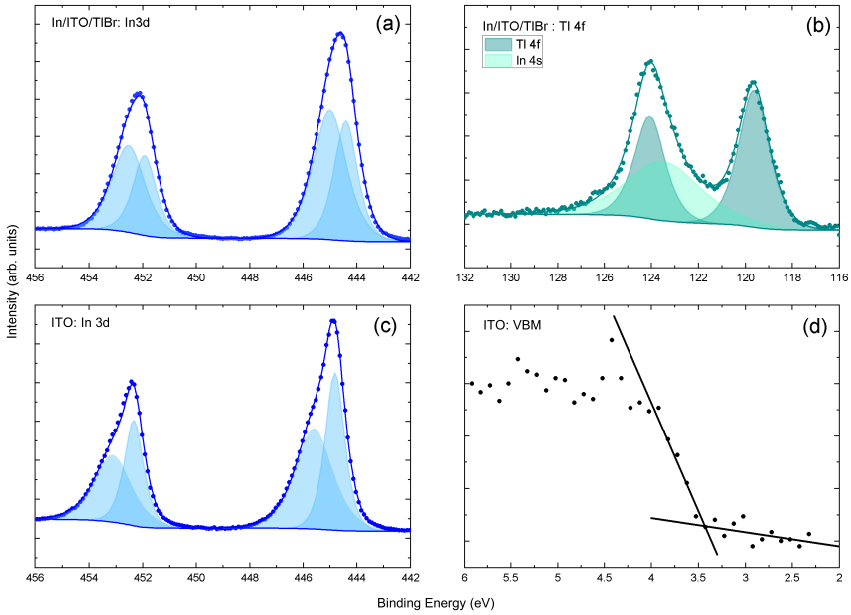


FIG. 4. (a) In 3$d$ core level peaks and (c) Tl 4$f$ core level peaks for the ITO/TlBr sample as well as the (b) In 3$d$ core level peak and (d) valence band photoemission spectrum for the thick ITO sample.

TABLE II. Binding energy and full width at half maximum (FWHM) of the core level peaks and valence band photoemission extrapolations used to fit the XPS data shown in Figures 1, 2, 3 and 4.

| **Sample** | **Region** | **Component** | **Binding Energy (eV)** | **FWHM (eV)** |
|---|---|---|---|---|
| TlBr | Tl 4f | TlBr | 118.94 ± 0.05 | 0.83 |
| | Br 3p | TlBr | 181.69 ± 0.05 | 1.87 |
| | VBM | ... | 1.6 ± 0.1 | ... |
| In/TlBr | Tl 4f | TlBr | 119.68 ± 0.05 | 1.01 |
| | | $Tl_2O_3$ | 117.90 ± 0.05 | 0.54 |
| | | In 4s | 123.80 ± 0.05 | 3.8 |
| | Br 3p | TlBr | 182.33 ± 0.05 | 1.89 |
| $SnO_2$/TlBr | Tl 4f | TlBr | 119.51 ± 0.05 | 1.30 |
| | | In 4s | 123.67 ± 0.05 | 4.28 |
| | Sn 3d | $SnO_2$ | 487.13 ± 0.05 | 1.14 |
| | | CBP | 487.65 ± 0.05 | 1.26 |
| ITO/TlBr | Tl 4f | TlBr | 119.64 ± 0.05 | 1.53 |
| | | In 4s | 123.46 ± 0.05 | 3.67 |
| | In 3d | $In_2O_3$ | 444.41 ± 0.05 | 1.03 |
| | | CBP | 445.01 ± 0.05 | 1.44 |
| Thick $SnO_2$ | Sn 3d | $SnO_2$ | 487.61 ± 0.05 | 1.56 |
| | | CBP | 487.03 ± 0.05 | 0.85 |
| | VBM | ... | 3.7 ± 0.1 | ... |
| Thick ITO | In 3d | $In_2O_3$ | 444.81 ± 0.05 | 0.85 |
| | | CBP | 445.60 ± 0.05 | 1.65 |
| | VBM | ... | 3.4 ± 0.1 | ... |

ric In/TlBr, In/$SnO_2$/TlBr and In/ITO/TlBr planar devices with a 5×5 $mm^2$ contact area are presented in Figure 6. All three devices exhibit an Ohmic response and leakage current <2.5 nA at 100 V. The bulk resistivity for the In/$SnO_2$, In/ITO contacted devices were found to be slightly lower than for In-only contacting: In/$SnO_2$/TlBr, (9.84 ± 0.10) $\times 10^{10}$ Ωcm; In/ITO/TlBr, (7.25 ± 0.12)$\times 10^{10}$ Ωcm; and In/TlBr, (1.06 ± 0.01)$\times 10^{11}$ Ωcm.

## IV. DISCUSSION

Metal electrodes are typically used to contact TlBr in radiation devices [10]. It has been suggested, however, that reactions of the anode material with migrating $Br^-$ ions leads to the formation of non-conducting metal bromides which ultimately degrades the performance of the device [3]. Metal oxides are an alternative to metal contacts owing to their low reactivity. Device lifetime tests presented in Ref. 13 have shown that ITO-contacted devices have stable operation over long periods of time under unidirectional bias, suggesting that the $Br^-$ ions do not readily react with this contact material.

Investigation into any new electrical contact must address the band alignment at the contact/TlBr interface and resulting electronic behaviour of the device. Ohmic contacts are typically used in high resistivity devices such as TlBr due to their low contact resistance and linear and

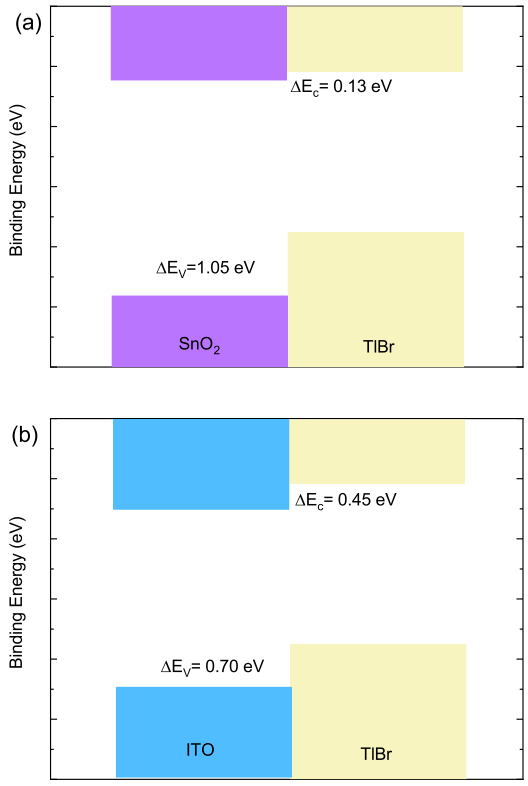


FIG. 5. The band offsets of the (a) $SnO_2$/TlBr and (b) ITO/TlBr heterojunctions at room temperature. The band gaps are 3.60 eV for $SnO_2$, 2.93 eV for ITO and 2.68 eV for TlBr. For both metal oxide contacts, a type-II staggered heterojunction is formed.

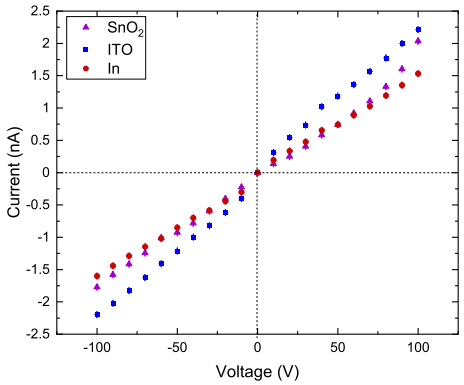


FIG. 6. Room temperature current voltage characteristics for 6.5×6.5×1.5 $mm^3$ symmetric with 5×5 $mm^2$ In/$SnO_2$, In/ITO and In contacted TlBr planar devices.

symmetric I-V relationships [24]. In order to achieve an Ohmic contact, the potential barrier at the contact/TlBr interface must be as small as possible.

Here, the Kraut method [14] was used to determine the conduction band offset at $SnO_2$/TlBr and ITO/TlBr interfaces. This can be used as a measure of the potential barrier formed when contacting, which was found to be 0.13 eV ± 0.17 eV and 0.45 ± 0.17 eV, respectively. Both values are smaller than the 0.80 eV barrier formed when TlBr is contacted with In metal, calculated by aligning the indium work function and electron affinity of TlBr, as shown in Figure 7 [25, 26].

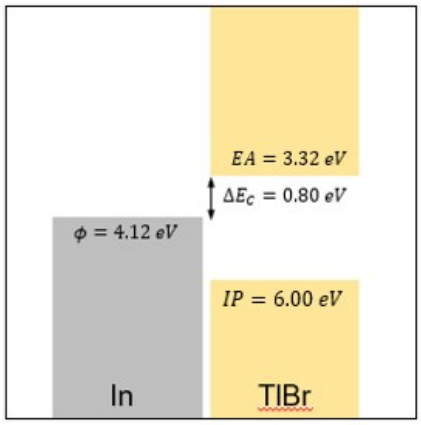


FIG. 7. The natural band alignment of indium and TlBr.

The I-V relationships for symmetric In/$SnO_2$, In/ITO and In contacted devices are shown in Figure 6. The resistivity values for each device satisfy the requirement for room temperature semiconductor detectors [27]. All three devices show near Ohmic responses, with very little non-linearity and a leakage current of less than 2.5 nA in the range -100 V to 100 V.

It is hypothesized that the use of metal oxide contacts, such as ITO or $SnO_2$, will result in a stable Ohmic device with increased lifetime, due to their low reactivity with $Br^-$ ions. Moreover, implementation of a symmetrical device structure, as shown in Figure 8, could allow for the use of bias switching to further increase the lifetime of the detector. This would need to be performed at a lower rate than when only metal contacts are used, due to the low reactivity of the metal oxides.

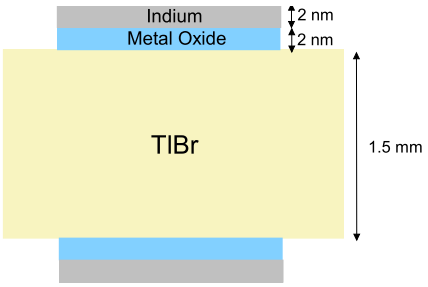


FIG. 8. Schematic diagram showing a symmetric In/metal oxide/TlBr device.

## V. CONCLUSION

In summary, planar TlBr devices with $SnO_2$ and ITO electrodes were investigated using XPS. It was found that both the $SnO_2$/TlBr and ITO/TlBr interfaces form type-II staggered heterojunction upon contacting. By using the Kraut method of valence band offset determination, the valence band offset of $SnO_2$/TlBr and ITO/TlBr heterojunctions were determined to be 1.05 ± 0.17 eV and 0.70 ± 0.17 eV, respectively. The corresponding conduction band offsets were then found to be 0.13 ± 0.17 eV and 0.45 ± 0.17 eV respectively. The potential formed by the conduction band offset was found to be lower than that of an In/TlBr junction. The I-V relationship of symmetric In/$SnO_2$/TlBr and In/ITO/TlBr planar devices are Ohmic and similar to In/TlBr devices in the range -100 V to 100 V. Metal oxides are typically less reactive than pure metals. This, combined with the similar electronic response compared to indium contacts shown here, suggests that metal oxides have the potential to replace metal electrodes in the fabrication of TlBr radiation devices.

## VI. ACKNOWLEDGEMENTS

The Engineering and Physical Sciences Research Council is acknowledged for the funding of OKV's PhD studentship within the Next Generation Nuclear Centre for Doctoral Training (Grant No. EP/L015390/1). The XPS data collection was performed at the EPSRC National Facility for XPS ("HarwellXPS"), operated by Cardiff University and University College London, under Contract No. PR16195.

## VII. DATA AVAILABILITY STATEMENT

The data that support the findings of this study are available within the article.

[1] K. Hitomi, T. Shoji, and K. Ishii, Journal of Crystal Growth **379**, 93 (2013).
[2] V. Kozlov, M. Kemmel, M. Vehkamäki, and M. Leskelä, Nucl. Instr. and Meth. A **576**, 10 (2007).
[3] K. Hitomi, Y. Kikuchi, T. Shoji, and K. Ishii, IEEE Transactions on Nuclear Science **56**, 1859 (2009).
[4] A. Datta, J. Fiala, P. Becla, and S. Motakef, APL Materials **5**, 106109 (2017).
[5] A. Datta, P. Becla, and S. Motakef, Nucl. Instr. and Meth. A **784**, 37 (2015).
[6] L. F. Voss, A. M. Conway, R. T. Graff, P. R. Beck, R. J. Nikolic, A. J. Nelson, S. A. Payne, H. Kim, L. Cirignano, and K. Shah (2010) pp. 3746–3748.
[7] M. Shorohov, F. Muktepavela, L. Grigorjeva, K. Maniks, and D. Millers, Nucl. Instr. and Meth. A **607**, 120 (2009).
[8] J. B. Varley, A. M. Conway, L. F. Voss, E. Swanberg, R. T. Graff, R. J. Nikolic, S. A. Payne, V. Lordi, and A. J. Nelson, Phys. Stat. Solidi B **252**, 1266 (2015).
[9] A. J. Nelson, L. F. Voss, P. R. Beck, T. Graff, A. M. Conway, R. J. Nikolik, S. A. Payne, J.-S. Lee, H. Kim, L. Cirignano, and K. Shah, J. Appl. Phys **113**, 143713 (2013).
[10] V. Kozlov, M. Leskelä, M. Vehkamäki, and H. Sipilä, Nucl. Instr. and Meth. A **573**, 212 (2007).
[11] A. Datta, P. Becla, and S. Motakef, Proc. SPIE **10762**, 107620X (2018).
[12] A. Datta, P. Becla, and S. Motakef, IEEE Transactions on Nuclear Science **65**, 2329 (2018).
[13] A. Datta, P. Becla, and S. Motakef, Scientific Reports **9**, 9933 (2019).
[14] E. A. Kraut, R. W. Grant, J. Waldrop, and S. P. Kowalczyk, Phys. Rev. **44**, 1620 (1980).
[15] CRC Handbook, *CRC Handbook of Chemistry and Physics, 89th Edition* (CRC Press, 2008).
[16] G. E. McGuire, G. K. Schweitzer, and T. A. Carlson, Inorganic Chemistry **12**, 2450 (1973).
[17] P. Glans, T. Learmonth, K. E. Smith, J. Guo, A. Walsh, G. W. Watson, F. Terzi, and R. Egdell, Phys. Rev. B **71**, 235109 (2005).
[18] R. G. Egdell, J. Rebane, T. J. Walker, and D. S. L. Law, Phys. Rev. B **59**, 1792 (1999).
[19] R. G. Egdell, T. J. Walker, and G. Beamson, J. Electron Spectrosc. Relat. Phenom. **128**, 59 (2003).
[20] J. F. Moulder, W. F. Stickle, P. E. Sobol, and K. D. Bomben, *Handbook of X-ray Photoelectron Spectroscopy* (Perkin-Elmer Corporation, 1992).
[21] J. E. N. Swallow, B. A. D. Williamson, T. J. Whittles, M. Birkett, T. J. Featherstone, N. Peng, A. Abbott, K. J. Cheetham, P. Warren, D. O. Scanlon, V. R. Dhanak, and T. D. Veal, Adv. Funct. Mater **28**, 1701900 (2017).
[22] P. D. C. King, T. D. Veal, F. Fuchs, C. Y. Wang, D. J. Payne, A. Bourlange, H. Zhang, G. R. Bell, V. Cimalla, O. Ambacher, R. G. Egdell, F. Bechstedt, and C. F. McConville, Phys. Rev. B **79**, 205211 (2009).
[23] K. Reimann and M. Steube, Solid State Commun. **105**, 649 (1998).
[24] A. Owens, *Compound Semiconductor Radiation Detectors* (CRC Press, 2016).
[25] A. Terenin, Phys. Rev **36**, 147 (1930).
[26] H. B. Michaelson, J. Appl. Phys **48**, 4729 (1977).
[27] A. Owens and A. Peacock, Nucl. Instr. and Meth. A **531**, 18 (2004).

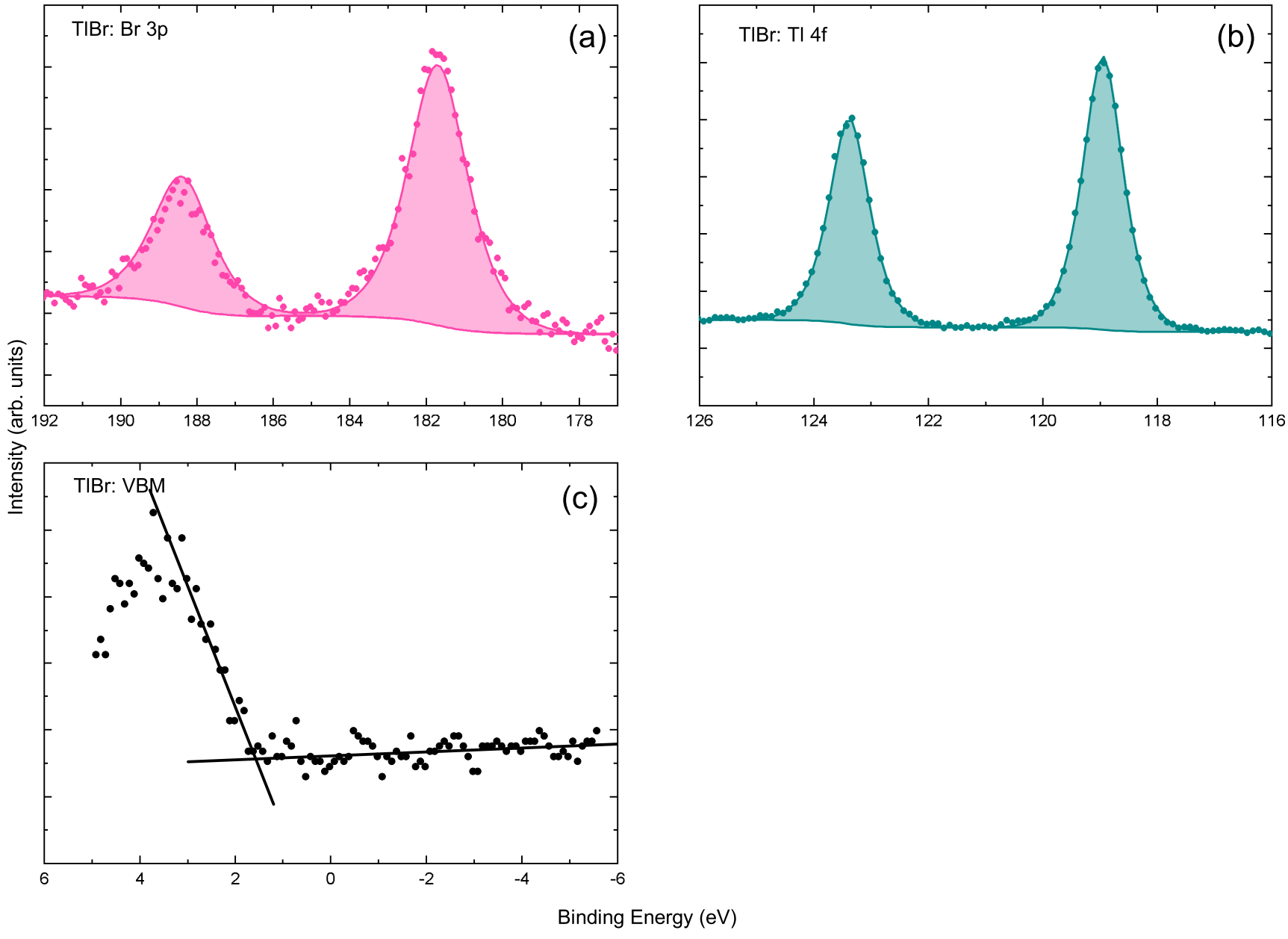
TlBr: Br 3p
(a)
TlBr: Tl 4f
(b)
TlBr: VBM
(c)
Intensity (arb. units)
192
190
188
186
184
182
180
178
126
124
122
120
118
116
6
4
2
0
-2
-4
-6
Binding Energy (eV)

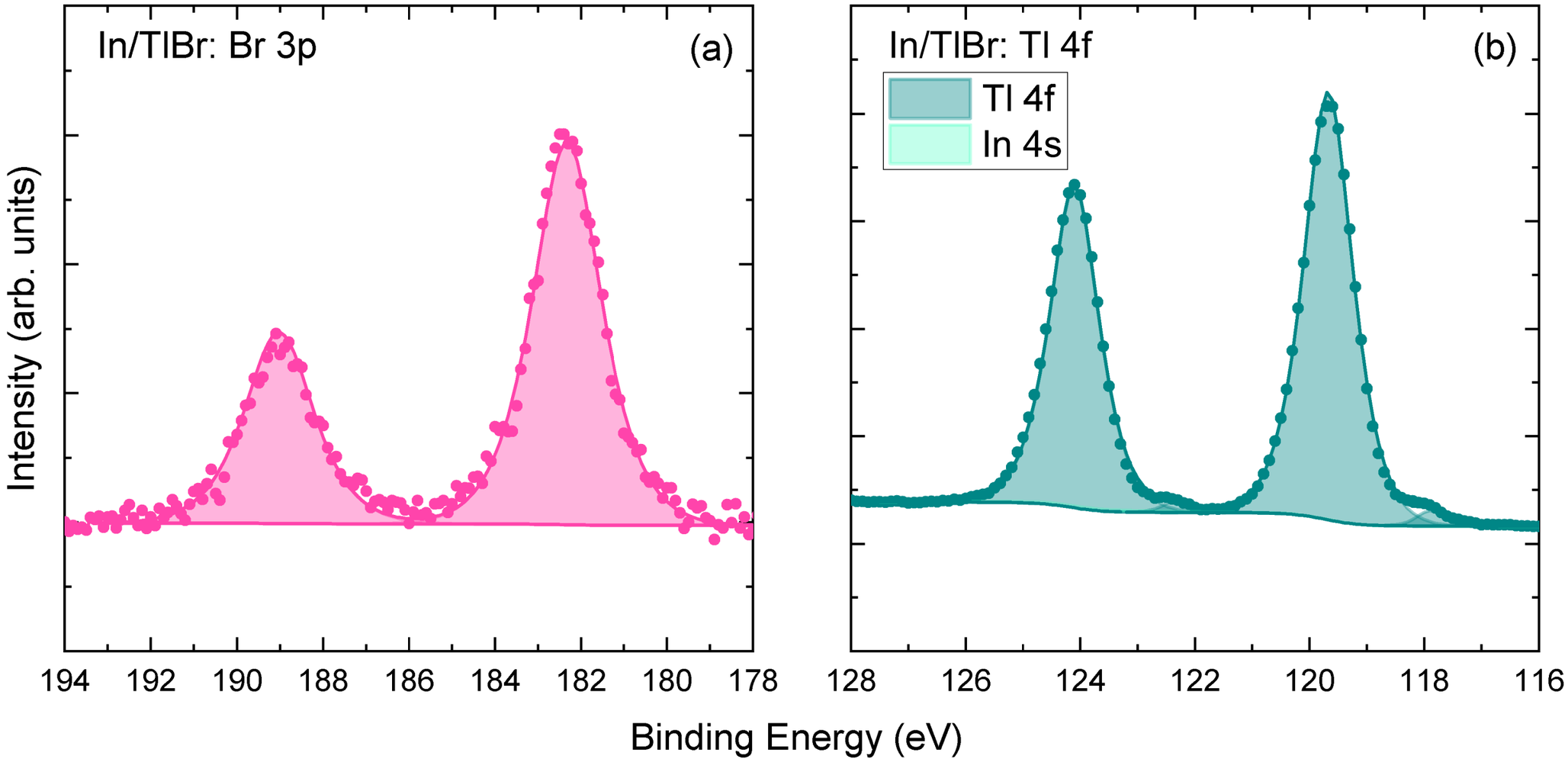
In/TlBr: Br 3p
(a)
In/TlBr: Tl 4f
(b)
Tl 4f
In 4s
Intensity (arb. units)
194
192
190
188
186
184
182
180
178
128
126
124
122
120
118
116
Binding Energy (eV)

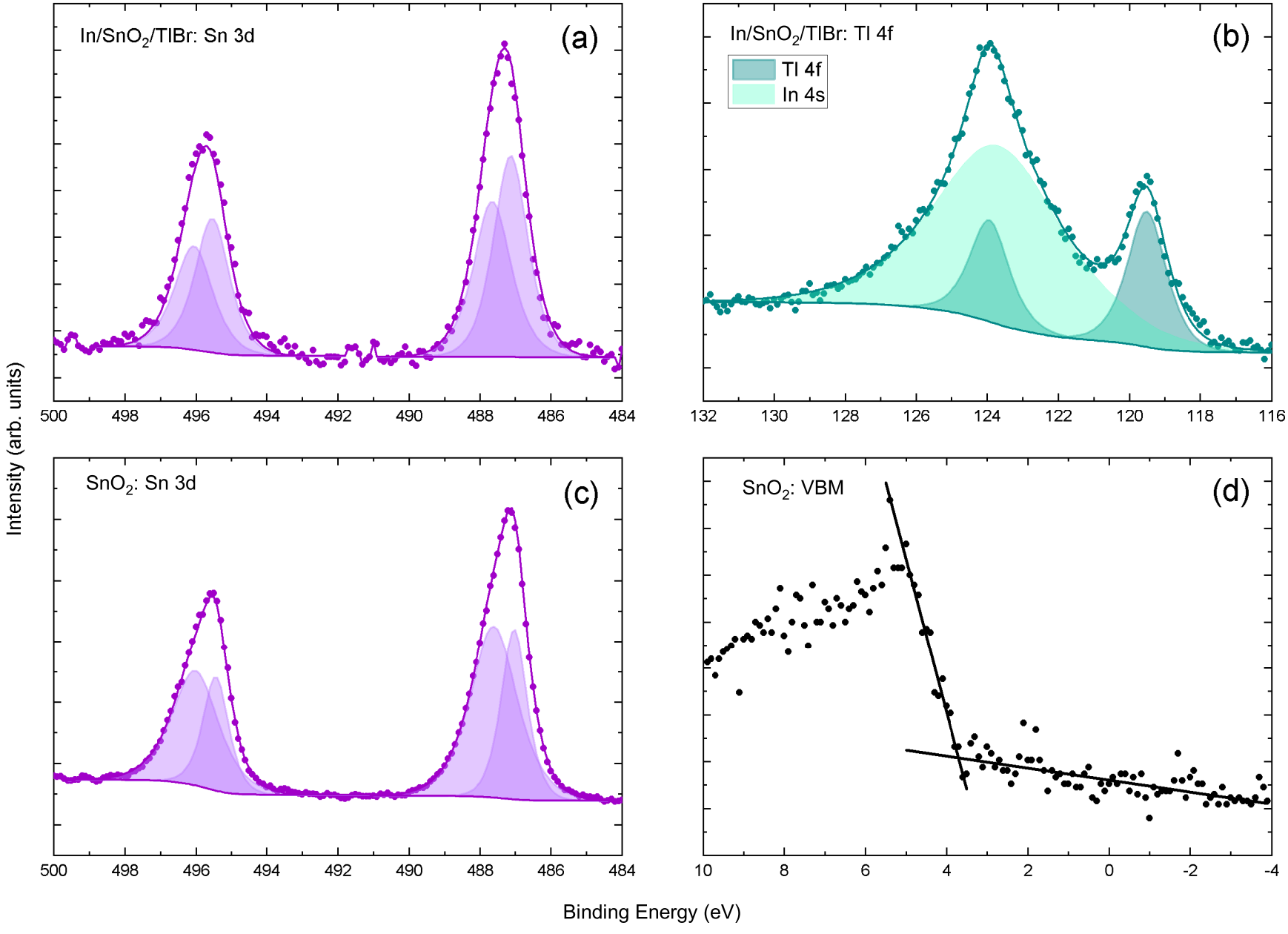
In/SnO2/TlBr: Sn 3d
(a)
In/SnO2/TlBr: Tl 4f
(b)
Tl 4f
In 4s
SnO2: Sn 3d
(c)
SnO2: VBM
(d)
Intensity (arb. units)
Binding Energy (eV)
500
498
496
494
492
490
488
486
484
132
130
128
126
124
122
120
118
116
10
8
6
4
2
0
-2
-4

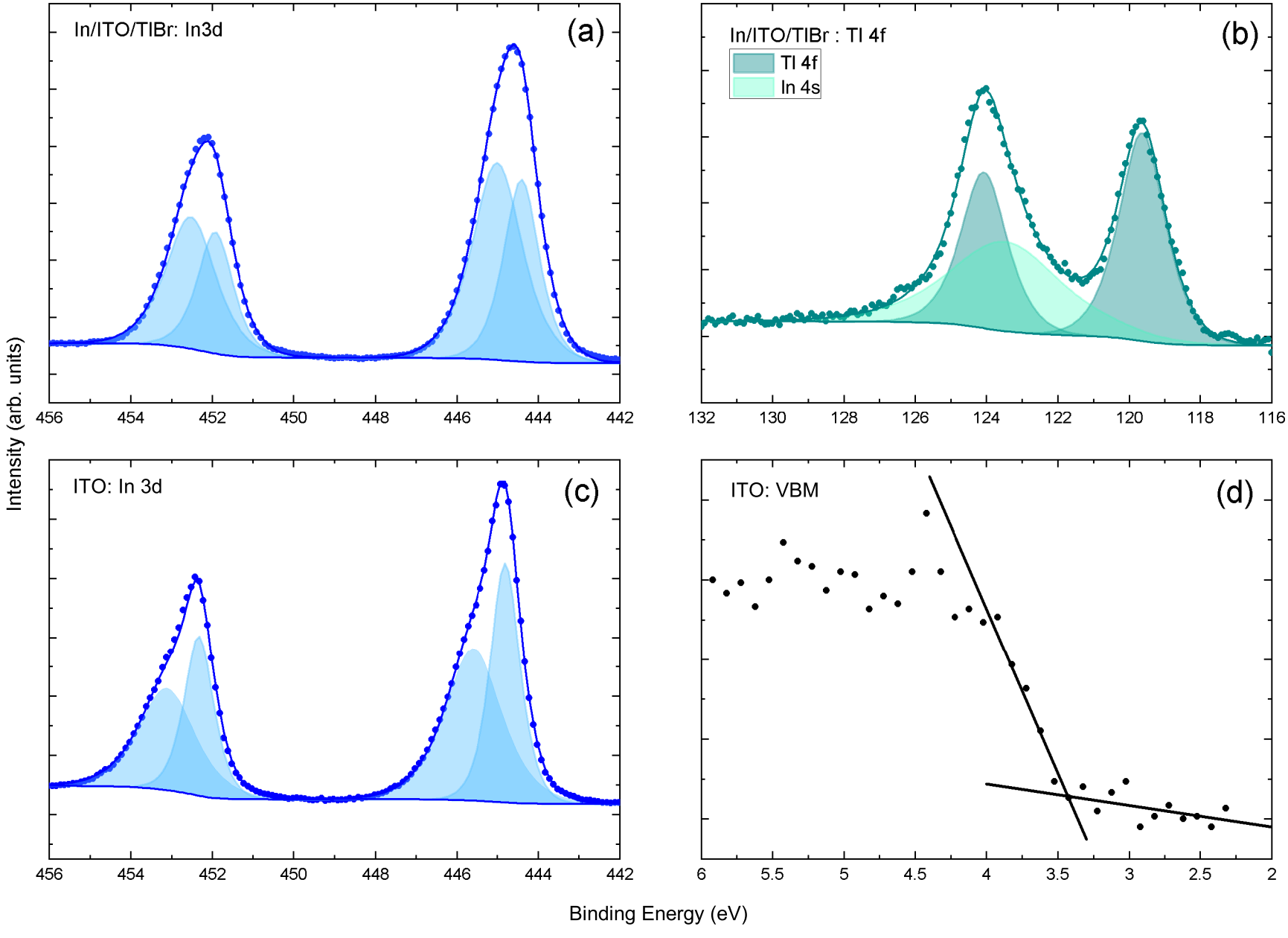
In/ITO/TlBr: In3d
(a)
In/ITO/TlBr : Tl 4f
(b)
Tl 4f
In 4s
ITO: In 3d
(c)
ITO: VBM
(d)
Intensity (arb. units)
Binding Energy (eV)
456
454
452
450
448
446
444
442
132
130
128
126
124
122
120
118
116
6
5.5
5
4.5
4
3.5
3
2.5
2

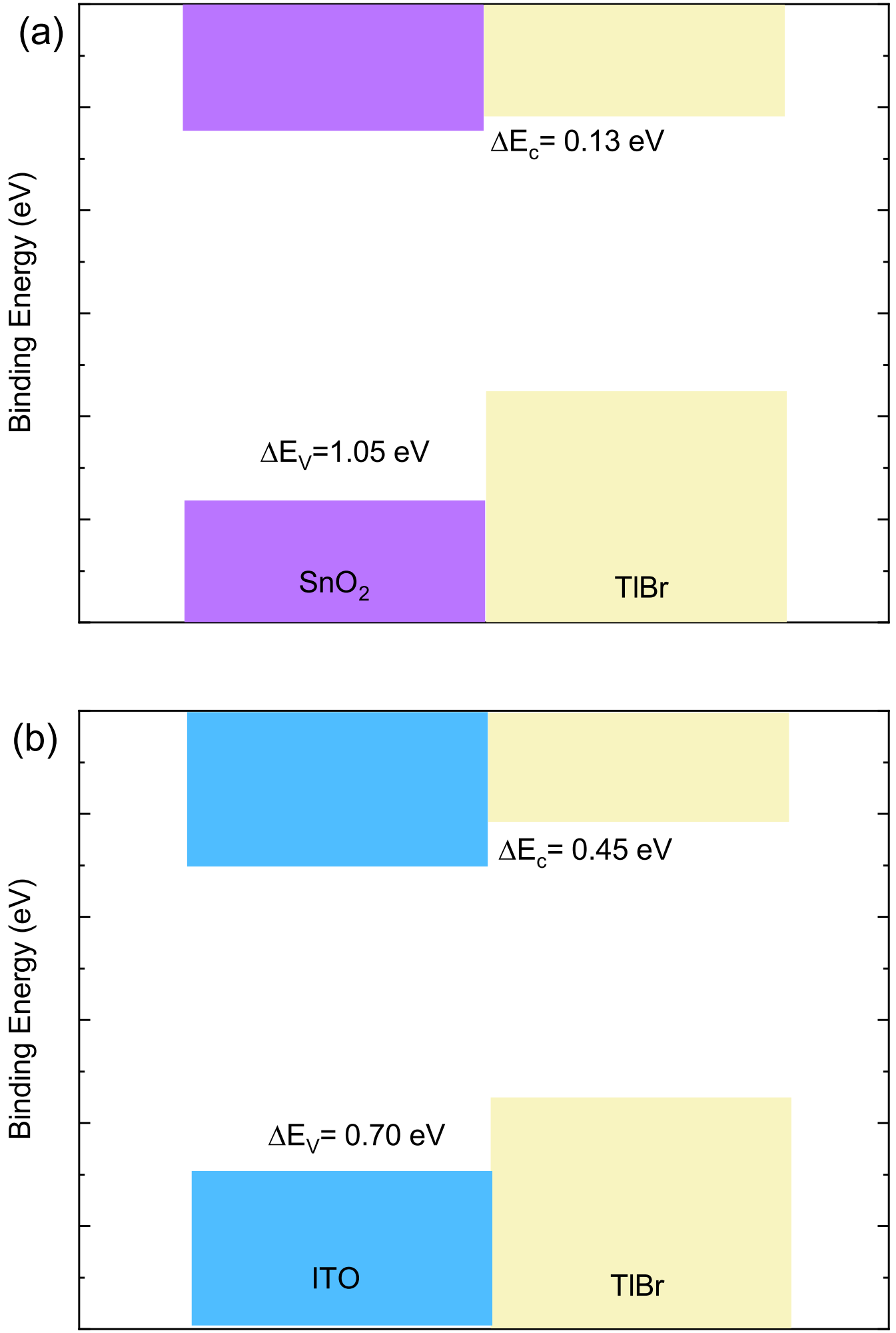
(a)
Binding Energy (eV)
ΔE_c= 0.13 eV
ΔE_V=1.05 eV
SnO_2
TlBr
(b)
Binding Energy (eV)
ΔE_c= 0.45 eV
ΔE_V= 0.70 eV
ITO
TlBr

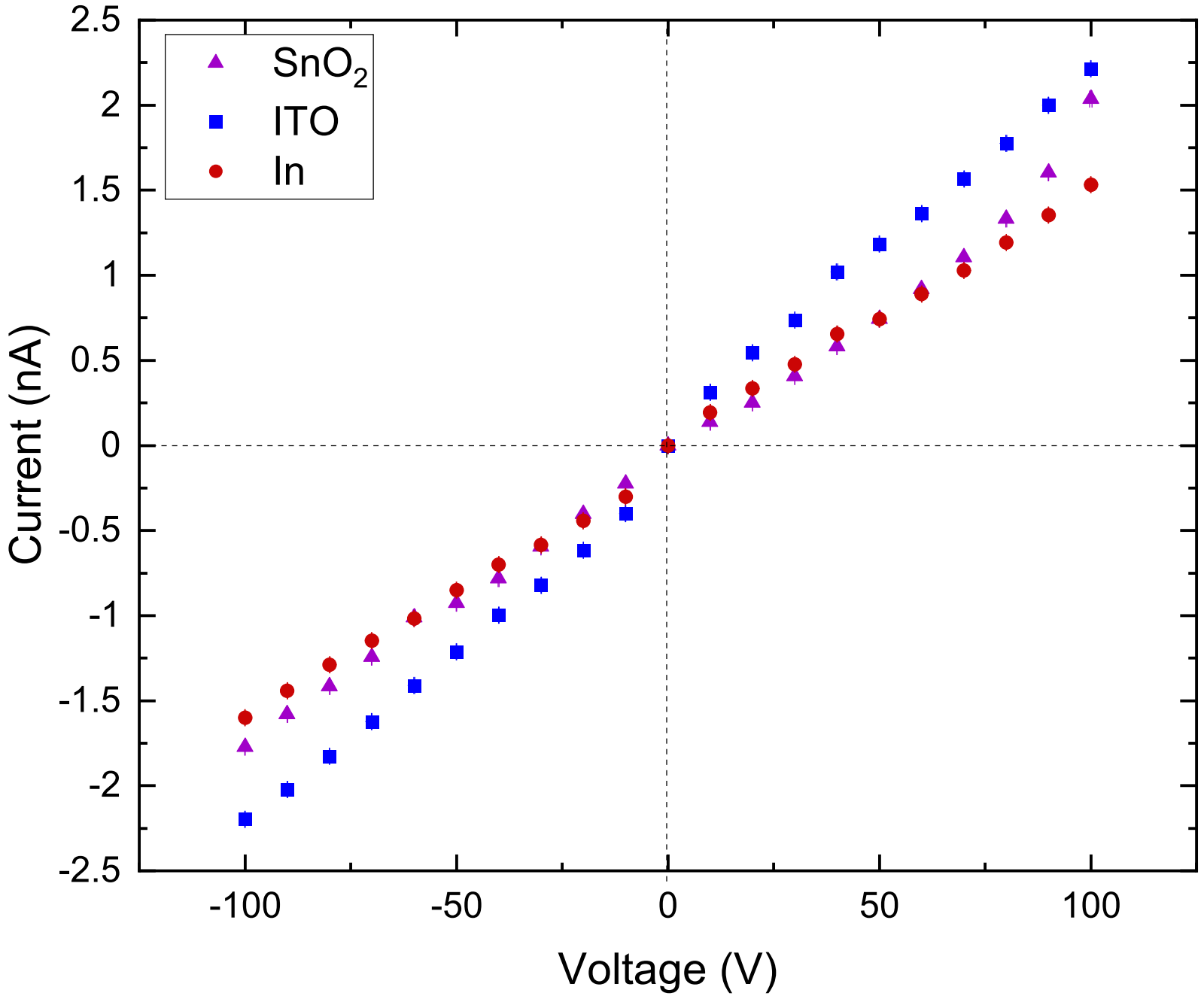
SnO2
ITO
In
Current (nA)
Voltage (V)
2.5
2
1.5
1
0.5
0
-0.5
-1
-1.5
-2
-2.5
-100
-50
0
50
100

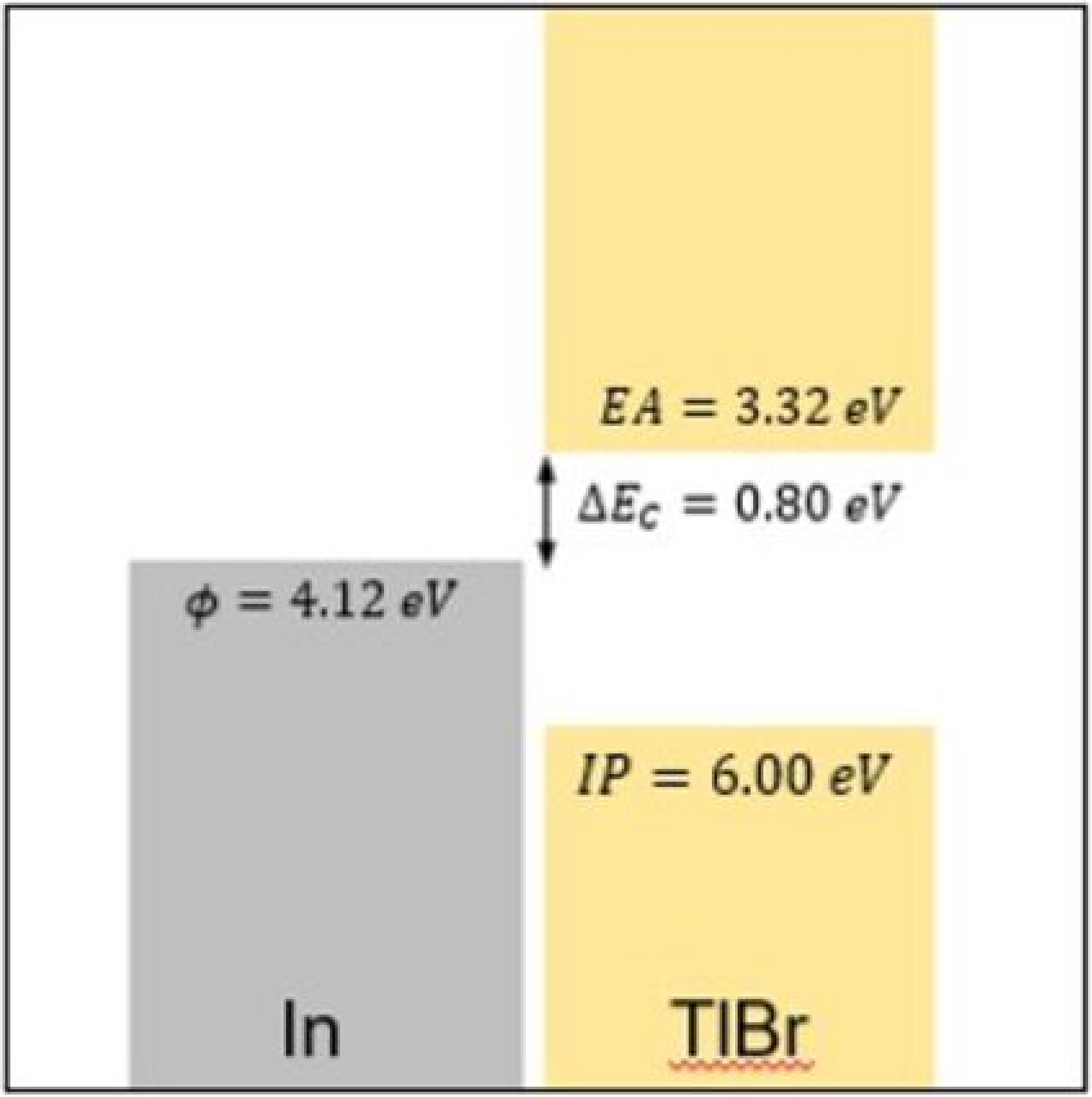
$EA = 3.32\ eV$
$\Delta E_C = 0.80\ eV$
$\phi = 4.12\ eV$
$IP = 6.00\ eV$
In
TlBr

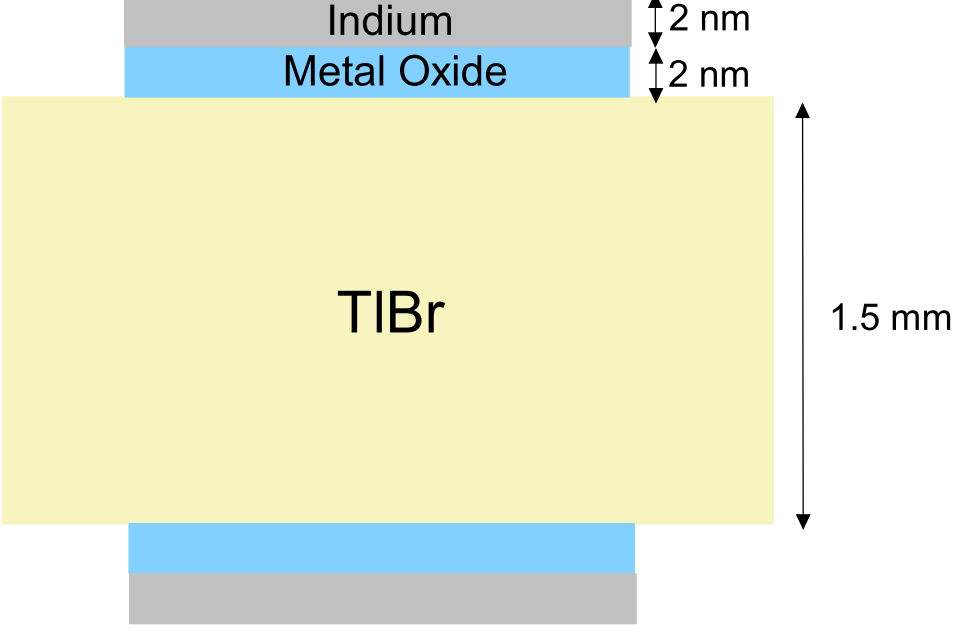
Indium
2 nm
Metal Oxide
2 nm
TlBr
1.5 mm